AD-A226 336

DTIC FILE COPY

A QUANTUM-EFFICIENT SYSTEMATICS-FREE PHOTON-COUNTING OPTICAL IMAGING SYSTEM FOR LONG BASELINE INTERFEROMETRIC IMAGING OF FAINT DEEP SPACE OBJECTS

University of Arizona

DTIC
ELECTE
SEP.10.1990
S B D

APPROVED FOR PUBLIC RELEASE; DISTRIBUTION UNLIMITED.

90 09 07 030

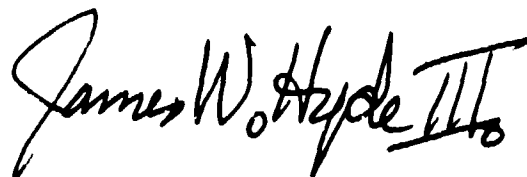RADC-TR-90-150 has been reviewed and is approved for publication.

APPROVED:

PAUL L. REPAK
Project Engineer

APPROVED:

FRED J. DEMMA, Acting Director
Directorate of Surveillance

FOR THE COMMANDER:

JAMES W. HYDE III
Directorate of Plans & Programs

DESTRUCTION NOTICE - For classified documents, follow the procedures in DOD 5200.22-M, Industrial Security Manual, or DOD 5200.1-R, Information Security Program Regulation. For unclassified, limited documents, destroy by any method that will prevent disclosure of contents or reconstruction of the document.

If your address has changed or if you wish to be removed from the RADC mailing list or if the addressee is no longer employed by your organization, please notify RADC (OCSP), Griffiss AFB NY 13441-5700. This will assist us in maintaining a current mailing list.

Do not return copies of this report unless contractual obligations or notices on a specific document requires that it be returned.

This report has been reviewed by the RADC Public Affairs Office (PA) and is releasable to the National Technical Information Service (NTIS). At NTIS it will be releasable to the general public, including foreign nations.

RADC TR-90-150 has been reviewed and is approved for publication.
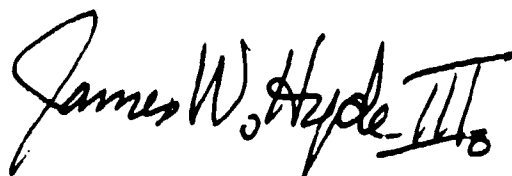
APPROVED:

PAUL L. REPAK
Project Engineer

APPROVED:

FRED J. DEMMA, Acting Director
Directorate of Surveillance

FOR THE COMMANDER:

JAMES W. HYDE III
Directorate of Plans and Programs

REPORT DOCUMENTATION PAGE

Public reporting burden for this collection of information is estimated to average 1 hour per response, including the time for reviewing instructions, searching existing data sources, gathering and maintaining the data needed, and reviewing the collection of information. Send comments regarding this burden estimate or any other aspect of this collection of information, including suggestions for reducing this burden, to Washington Headquarters Services, Directorate for Information Operations and Reports, 1215 Jefferson Davis Highway, Suite 1204, Arlington, VA 22202-4302, and to the Office of Information and Regulatory Affairs, Office of Management and Budget, Washington, DC 20503.

1. AGENCY USE ONLY (Leave Blank)	2. REPORT DATE	3. REPORT TYPE AND DATES COVERED
	June 1990	Final Jul 87 - Sep 89

4. TITLE AND SUBTITLE	5. FUNDING NUMBERS
A QUANTUM-EFFICIENT SYSTEMATICS-FREE PHOTON-COUNTING OPTICAL IMAGING SYSTEM FOR LONG BASELINE INTERFEROMETRIC IMAGING OF FAINT DEEP SPACE OBJECTS	C - F30602-85-C-0313 PE - 62301E PR - D174 TA - 15 WU - 05

6. AUTHOR(S)	
E. Keith Hege	

7. PERFORMING ORGANIZATION NAME(S) AND ADDRESS(ES)	8. PERFORMING ORGANIZATION REPORT NUMBER
University of Arizona Steward Observatory Tucson AZ 85721	

9. SPONSORING/MONITORING AGENCY NAME(S) AND ADDRESS(ES)	10. SPONSORING/MONITORING AGENCY REPORT NUMBER
Defense Advanced Research Projects Agency 1400 Wilson Blvd Arlington VA 22209-2308 Rome Air Development Center (OCSP) Griffiss AFB NY 13441-5700	RADC-TR-90-150

11. SUPPLEMENTARY NOTES

RADC Project Engineer: Paul L. Repak/OCSP/(315) 330-4481

12a. DISTRIBUTION/AVAILABILITY STATEMENT	12b. DISTRIBUTION CODE
Approved for public release; distribution unlimited.	

13. ABSTRACT (Maximum 200 words)

The objective was to demonstrate a prototype system for evaluation of image intensifier capabilities in speckle imaging applications and an observing system optimized for use in diffraction and statistics limited imaging at the lowest possible photon flux with the highest possible photon-counting efficiency. A four stage Proxitronic image intensifier system with digital video readout was developed for use as a high detective quantum efficiency photon-counting imaging detector optimized for long baseline speckle interferometric imaging of deep space objects.   Accurate noise bias calibration requires low geometric distortion image intensifiers as well as linear video readout to yield a stable, calibratable photon point spread function.   The image intensifier optimization is not limited to video raster systems but is intended to produce techniques for implementation of a fast phosphor (X-3 response) image intensifier first-stage with MAMA- or PAPA-type photon-coordinate readout systems.

14. SUBJECT TERMS		15. NUMBER OF PAGES
Image Intensifiers, Photon Counting Digital Video Processors Speckle Interferometric Imaging Systems		48
		16. PRICE CODE

17. SECURITY CLASSIFICATION OF REPORT	18. SECURITY CLASSIFICATION OF THIS PAGE	19. SECURITY CLASSIFICATION OF ABSTRACT	20. LIMITATION OF ABSTRACT
UNCLASSIFIED	UNCLASSIFIED	UNCLASSIFIED	UL

NSN 7540-01-280-5500

A QUANTUM-EFFICIENT SYSTEMATICS-FREE PHOTON-COUNTING OPTICAL IMAGING SYSTEM FOR LONG BASELINE INTERFEROMETRIC IMAGING OF FAINT DEEP SPACE OBJECTS

Stephen O. Davis
Al Miller
Dickey Hitchcock

Table of Contents

List of Figures

A QUANTUM-EFFICIENT SYSTEMATICS-FREE PHOTON-COUNTING OPTICAL IMAGING SYSTEM FOR LONG BASELINE INTERFEROMETRIC IMAGING OF FAINT DEEP SPACE OBJECTS

E. Keith Hege

Steward Observatory
University of Arizona
Tucson, AZ 85721

ABSTRACT

We have developed a four stage Proxitronic® image intensifier system with digital video readout for use as a high detective quantum efficiency photon-counting imaging detector optimized for long baseline speckle interferometric imaging of deep space objects. Accurate noise bias calibration requires low geometric distortion image intensifiers as well as linear video readout to yield a stable, calibratable photon point spread function. The image intensifier optimization is not limited to video raster systems but is intended to produce techniques for implementation of a fast phosphor (X-3 response) image intensifier first-stage with MAMA- or PAPA-type photon-coordinate readout systems. The objective is to demonstrate a prototype system for further evaluation of image intensifier capabilities in speckle imaging applications, and to demonstrate an observing system optimized for use in diffraction- and statistics-limited imaging at the lowest possible photon flux with the highest possible photon-counting efficiency.

1. Introduction

Most applications which require large astronomical telescopes are limited by the available signal (photon flux). Post detection high angular resolution imaging applications are further limited by the atmospheric correlation time to very short primary integrations. Narrow bandpass short exposure specklegrams with less than one photon per pixel, on the average, must be detectable. The only sufficiently noise free imagers presently available are image intensifiers. These in turn need low-noise linear readout systems.

These intensified image detectors are carried by large astronomical telescopes at the focal plane of astronomical instrumentation, which normally operates in the dark telescope chamber at night time ambient temperatures. Remote instrument support capabilities are located away from the telescope, and in a more suitable work environment. This requires conversion of the signal to digital format for noise free transmission. For greatest noise immunity, the analog to digital conversion is close to the primary detector.

There must be provision for real-time viewing of the data stream, both for object acquisition

as well as for telescope guiding.

For evaluation of the quality of the data, some near real-time "quick look" capability is required to evaluate the quality of the results to be expected from the off-line complex process required for diffraction- and statistics-limited image construction. This requires significant image construction capability at the observing site.

Because the sophisticated post-detection image construction algorithms require the raw image data, real-time data logging is crucial. At the lowest light levels, simply recording the photoelectron event coordinates will suffice. At higher photon fluxes, where more than one event per pixel is detectable, the entire greyscale video data stream must be recorded.

The complexity of the instrumentation supported, and the requirements for considerable on-site data reductions and analysis capability defines the need for a high-speed real-time instrumentation host computing system. Integrated data driven telescope and instrumentation control is required in an optimized speckle imaging system.

2. The Low Light Level Detecting System

Figure 2.1   ProxyBlue. The Steward Observatory Four-stage Proxitronic Image Intensifier System with CCD readout. This unit contains the intensifier tubes, thermoelectric cooler, voltage divider, Kowa transfer lens assembly and Pulnix CCD image sensor.

Specklegrams are read at 60Hz to freeze the atmospheric perturbations. Imaging detectors scanned at such frame rates typically have several hundred electrons noise per pixel. A very

high gain image intensifier system is necessary to provide sufficient noise-free amplification for unambiguous, quantum-noise limited, detection of single photoelectron events.

Newly developed Proxitronic proximity focused image intensifier technology has been utilized to produce a four stage image intensifier package with minimum geometrical distortion, low noise, and high detective quantum efficiency. A photograph of the Steward Observatory Proxitronic Image Intensifier package "**ProxyBlue**" is shown in Fig. 2.1. The name reflects its spectral sensitivity, optimized for maximum quantum efficiency at blue to near ultraviolet wavelengths.
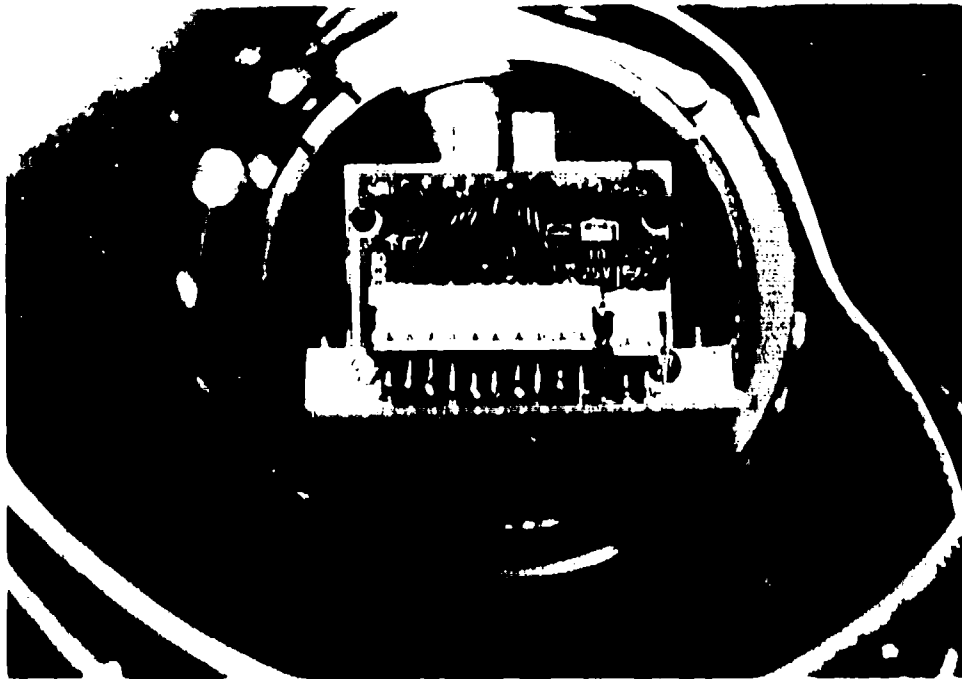
Figure 2.2   The Pulnix CCD image sensor mounted on the Kowa transfer lens assembly.

A Pulnix® video CCD sensor is transfer lens coupled to the output of the four stage image intensifier system with two fast Kowa® lenses operating as a fast 2:1 image reducer, as shown in Fig. 2.2. The primary video signal is obtained using the Pulnix camera electronics, Fig. 2.3, which has been modified to linearize the video output. To minimize noise, the A/D conversion system is mounted integrally with the CCD electronics. Normally the system operates synchronously with the digital processor at 60Hz, repeat field. But RS-170 30Hz interlaced field operation is switch selectable for certain laboratory test procedures.

A DTI-100 digital video processor, developed in collaboration with Peter R. Vokac of Digital Television Imagery, Inc., (Hege and Vokac 1986) allows capture of digital video data in formats suitable for full-frame greyscale image processing (bright objects) or for photoelectron event processing (faint objects). More than one photon per pixel is likely to be detected for objects of sufficient brightness. In this case it becomes necessary to record a video amplitude for each pixel (greyscale mode). For fainter objects a pixel rarely records even one photon and even more rarely multiple photons. In that case recording only the coordinates of pixels

which have detected photons provides nearly linear, noise free data compression (event mode).
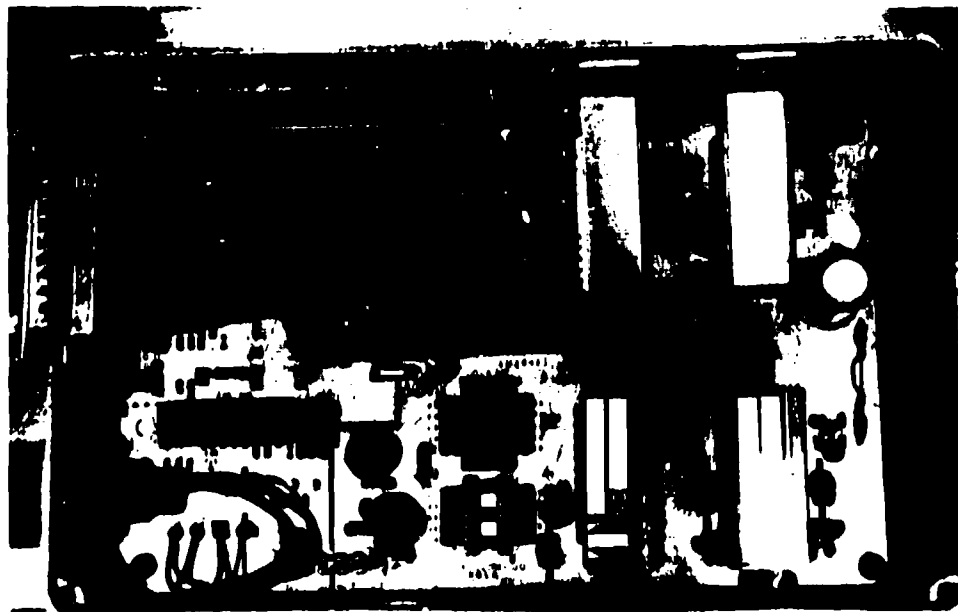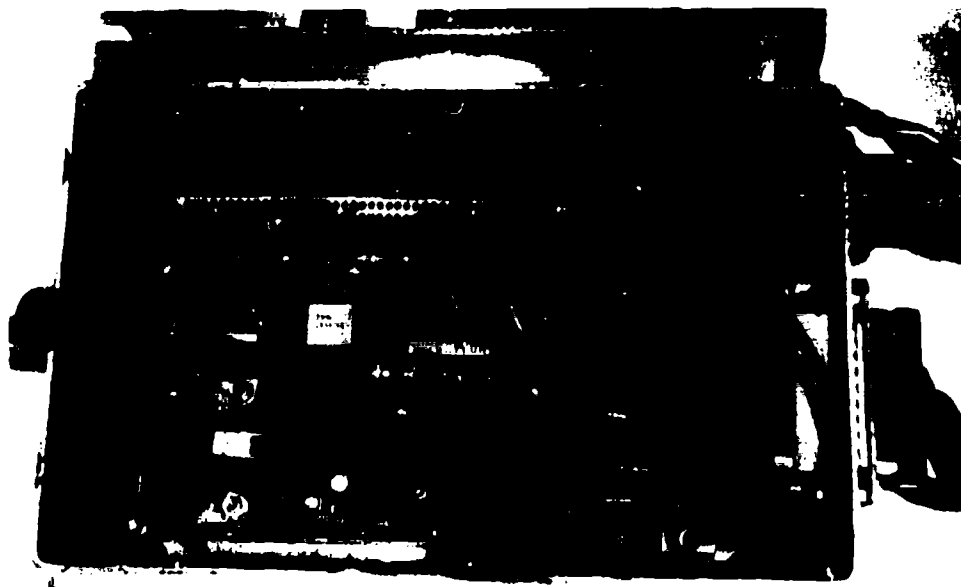
Figure 2.3   Video Preprocessing. The Pulnix Video Processor and the Analog-to-Digital Converter (above). The digital Taxi Sync receive and Data send (below).

Both bright and faint object mode data are digitally corrected to suppress time lag effects due to image decay time, which is dominated by P-20 phosphor afterglow in the image intensifier gain stages. The DTI-100 digital video processor is shown in Fig. 2.4.
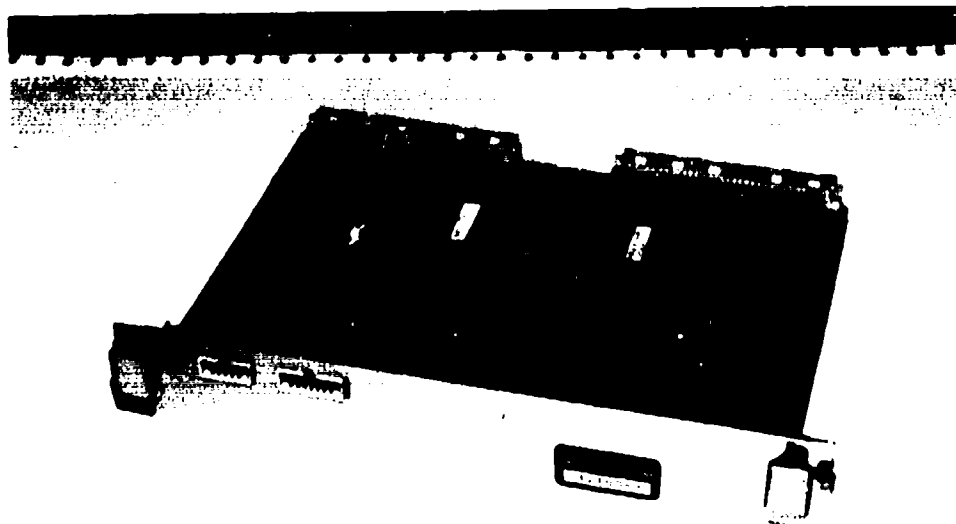
Figure 2.4 The DTI-100 Digital Video Processor. This 10MHz synchronous processor is wire wrapped in this prototype system.
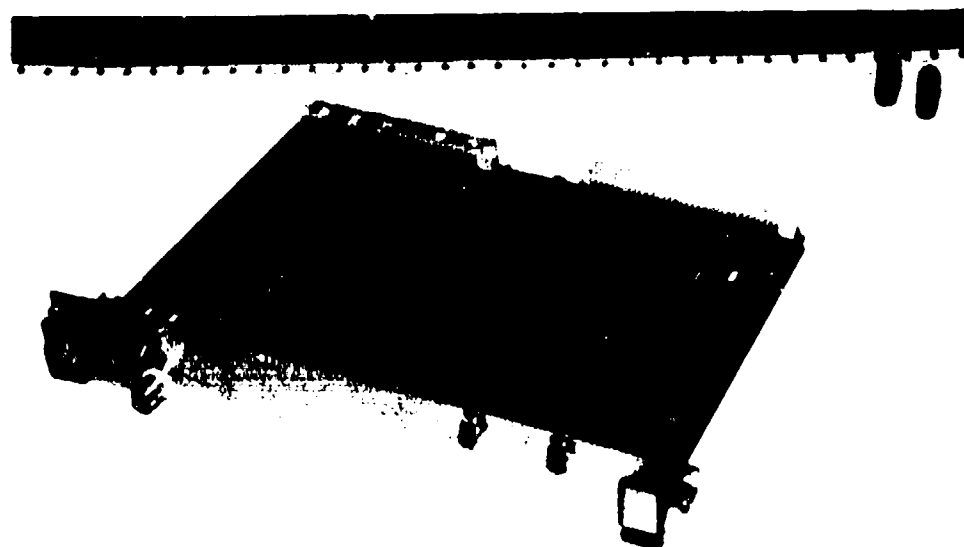
Figure 2.5 The DTI-100 VMEbus Interface Unit. This also contains a digital Taxi (Data receive and Sync send). This board is also wire wrapped.

The DTI-100 is integrated into the VMEbus host system with an AMD Taxi® data interface carrying the pixel synchronizing horizontal (H) and vertical (V) signals to the detector system

5

at the telescope and the digital video data (at 10Mbytes/s) from the digitizer at the telescope using fiber optics (Fig. 2.5). This unit also contains a D/A converter for output of RS-170 video to a conventional video monitor.
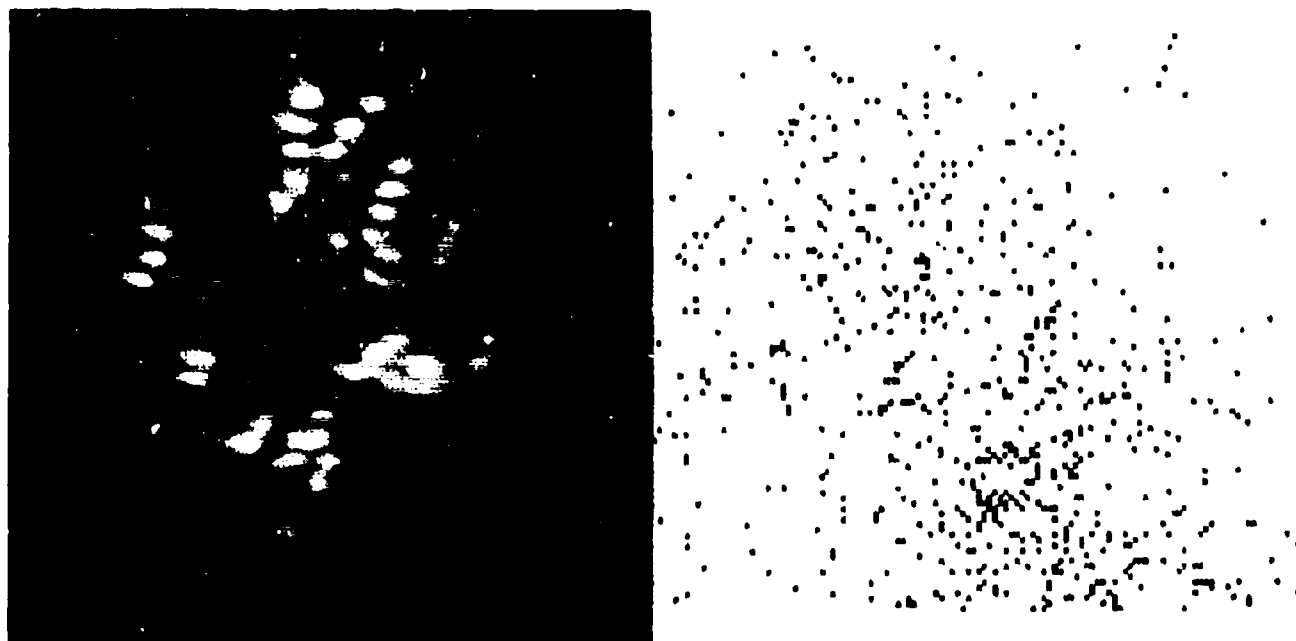
Figure 2.6   Examples of Greyscale (Capella — left) and Event (ADS11344 — right) Data. For the event data only the x- and y-coordinates of the photoelectron events are recorded.

For on-line image construction (events only in this prototype system), a "quick-look" image construction capability is implemented with an 18MHz floating point math-coprocessor Math-Cop2® from Io, Inc. Software is being developed for K-T cross-correlation accumulation as well as autocorrelation function accumulation. Recent progress with image construction algorithm development in collaboration with Queens University (Kingston, Ontario — Meng et al. 1989) suggests the possibility of using the more accurate triple correlation procedure in this processor.

System integration, which provides high-level software development and validation as well as telescope and instrumentation control capability, is accomplished with a Sun Microsystems 4/110 scientific workstation. The digital video processor is implemented in a VMEbus MC68000 hosted unit which operates as an extension of the Sun 4/110 VMEbus.

2.1 The Four-stage Proxitronic Image Intensifier

This system consists of four stages of Proxitronic proximity focused image intensifiers, the first stage having 100ns response X-3 phosphor output. The first stage was specifically selected using laboratory tests (Cromwell 1989) which showed that intensifier to have a photon-counting efficiency exceeding 80% of the measured first diode photocathode

efficiency. This yielded an overall photon-counting efficiency of 15% at its peak efficiency near 400nm.

A mechanical assembly was designed and fabricated to

> carry the image intensifiers at the instrumental focal plane.
> relay the intensified image to the image sensor.
> position the imager at the relayed intensified focal plane.
> house the voltage divider for the multi-stage intensifier.
> support the CCD image sensor.
> allow transfer lens focus adjustment.
> provide image intensifier photocathode cooling.
> connect dry air, high voltage and cooler power sources.
> interface temperature sensor, imager control and video data signals.

Fig. 2.7 illustrates these details.
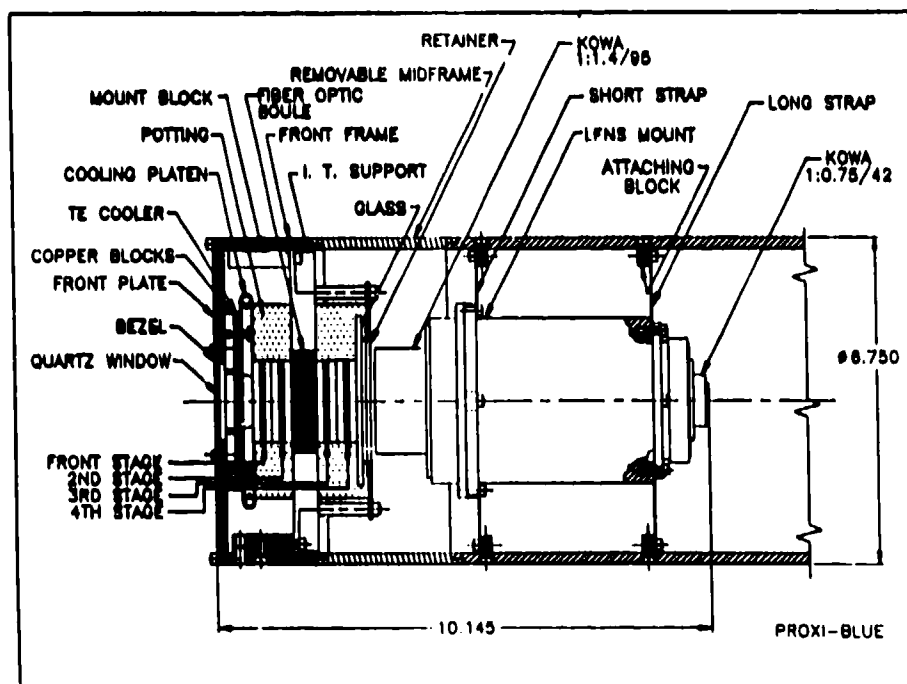
Figure 2.7 Mechanical layout of ProxyBlue image intensifier.

The image tube assembly consists of two two-stage subassemblies. These are separated by a fiber-optic boule, across which 30 KV is dropped, to allow 15KV/stage to be applied to each stage of a four stage intensifier using only a 30KV power supply. Lower voltage operation is crucial at the mountain top sites of large astronomical telescopes. A two-stage image tube subassembly, potted for high altitude high voltage operation, is shown in Fig. 2.8.

The transfer lens assembly consists of a pair of Kowa lenses operating as an f/1.4 2:1 image reducer. This maps the image intensifier point spread function onto the CCD imager at a scale at which the pixel size approximately matches the Nyquist sampling size. The effective

resolution, referred to the photocathode, is about 75 μm FWHM (about 13 lp/mm at 5% modulation).

Figure 2.8 Photograph of two-stage Proxitronic image tube subassembly.

A focus mechanism is provided to assure the sharpest possible point spread function in the very shallow depth of the f/0.75 Kowa focused image on the CCD image sensor. The remoted Pulnix CCD sensor head is mounted directly onto the image transfer lens assembly. The placement and alignment of the sensor is critical at this f/0.75 focus.

The RTV silicone potted voltage divider occupies the space surrounding the transfer lens.

A refrigerated liquid cooled copper platen provides cooling to the first stage photocathode. The thermoelectric cooler buffers the temperature gradient so that the quartz image intensifier input window is kept at ambient temperature. This provides a thermally neutral package with no heat load into the telescope chamber, which is essential to preserve image quality (seeing) at the telescope.

2.2 Pulnix Camera Modifications and the Analog-to-digital Converter

The requirement for optimum performance as a linear, low noise imager dictated some modifications to the standard Pulnix TM-540® RS-170 video imager. Some of the original on-board electronics provides image processing to improve cosmetic appeal and not to preserve linearity of response. We identified the point at which the linear CCD output signal can be extracted, amplified and applied to the analog-to-digital converter (ADC). Gain adjustment is provided to match the dynamic range of the linear video response to the sensitivity of

the ADC. To minimize noise, the ADC unit is mounted in close proximity to the camera electronics, with particular attention to grounding and rf shielding. Careful measurement of H- and V-synchronized pixel timing revealed that small, uniform phase drifts exist because the Pulnix system uses a non-integral 606.66 clock pulses per video line (including blanking interval). To prevent sample time dependent systematic readout noise, we use the camera pixel clock for constant pixel phase ADC timing control. The latched digital value is then transferred without pixel phase induced error. Precise system synchronization is achieved with 10ns stepwise adjustable 0 — 100ns (one CCD pixel time) delays.

2.3 *The DTI-100 Digital Video Processor*

The DTI-100 is the master controller for this pixel synchronous digital video processor. The schematic block diagram is shown in Fig. 2.9. The Pulnix imager is controlled in the conventional way, with H and V sync digitally computed from a crystal controlled timebase, to accurately synchronize the processor's logical pixels with the sensor's physical pixels. This avoids all systematic effects of pixel vs sample aliasing. To avoid propagation delay dependent synchronization errors, the digital delays are tuned to the particular set of data and control Taxi fiber optic lines which will be used with this system at all observing sites.

Data digitized in the "repeat field" 60Hz framing mode as 240 lines of 512 8-bit pixels per line is fed to the digital video processor. A digital filter coadds adjacent pixels in pairs to yield a 240 × 256 pixel format further enhancing the signal-to-noise ratio while providing a more convenient pixel aspect ratio.

A one-frame digital video delay (frame store) allows digital subtraction of the previous video field from the current video field, pixel by pixel, so that only new information arriving in the current field is captured. This full frame subtraction of the previous image from the current image provides image intensifier lag suppression, preventing multiple detection of photoelectron responses in more than one video frame. By running a shutter synchronously with the video framing, this feature can also be used for greyscale imaging: the afterglow in the previous field with the shutter closed provides the black (zero) level for the current field with the shutter open. A Uniblitz shutter is provided in both Steward Observatory speckle cameras (Hege *et al.* 1982 and Beckers *et al.* 1983) for this purpose.

Logic in the DTI-100 allows output of either the digitized video raster, with or without subtraction of previous frame (greyscale), or the coordinates of the detected photoelectrons (events) for each field.

At higher light levels the event detection scheme saturates if there is significant probability of more than one photon per pixel. In that case the pixel-by-pixel frame subtract capability provides lag-suppressed greyscale imaging. This mode of operation requires frame synchronized shuttering to provide dark subtracted zero-level (phosphor lag-induced image intensifier "afterglow") calibration.

For digital video logging, the system allows selection of both unsubtracted (raw) and frame subtracted (V-diff) linear greyscale data. For real-time display, the system also provides the

9

reconstructed event detected video.
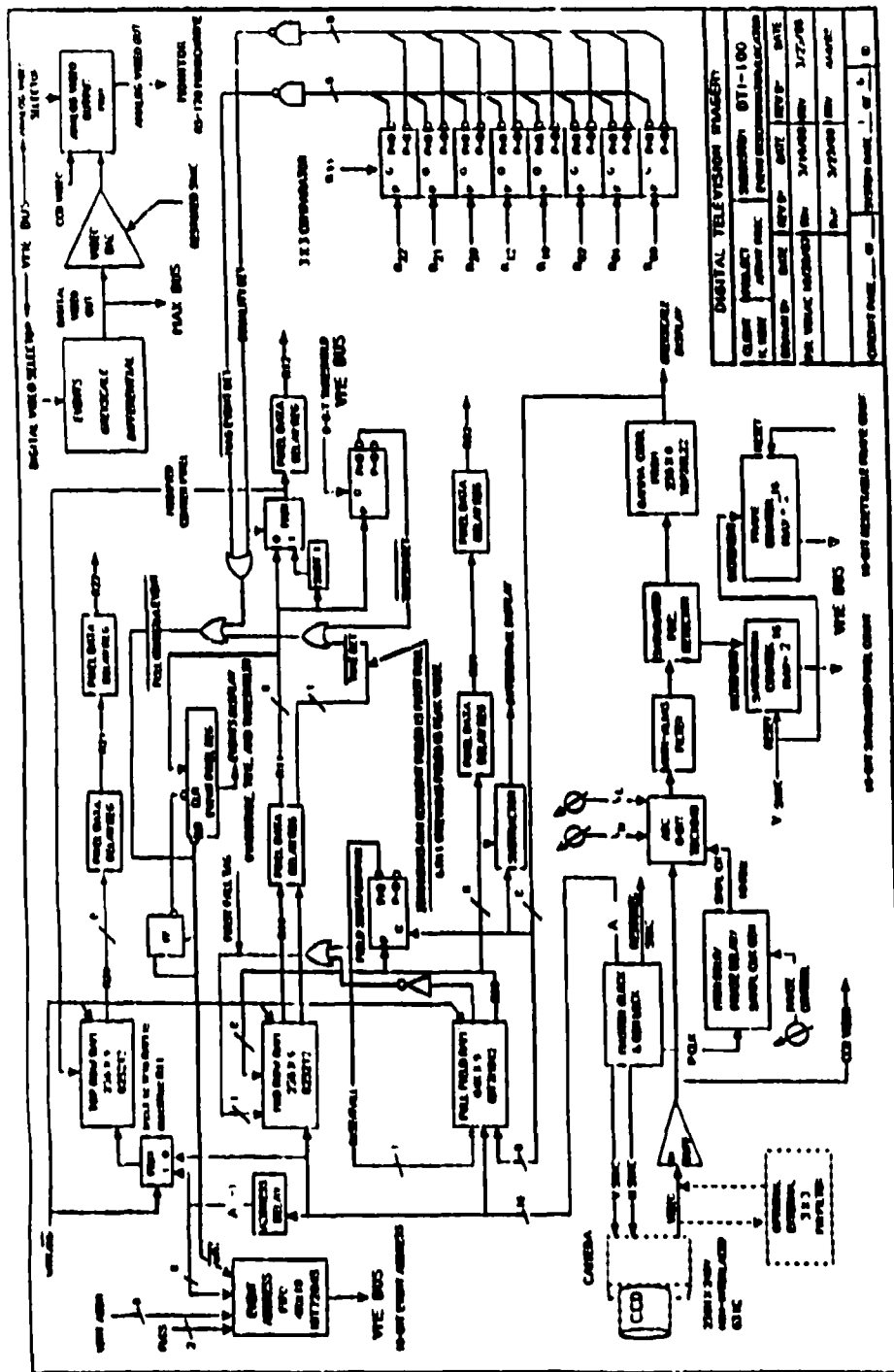
Figure 2.9   DTI-100 schematic block diagram.

10

The digital video logic provides thresholded localization of a peak to a unique pixel in a unique frame. The pixel coordinates are each 8 bits, H (=x) and V (=y). For each detected event these coordinates are loaded into a 16 bit wide 4096 bit deep FIFO memory for capture by the host computer. The detection logic operates by continuously inspecting a 3 × 3 subraster centered on (x-1, y-1) with respect to the location being tested. An event is detected if the pixel

> value exceeds a threshold.
> value is less than a second threshold.
> value is greater than that of its eight nearest neighbors.
> value is greater than its value in the previous or following field.
> address is greatest of nearest neighbors with equal values.

This scheme provides some immunity to ion events, which is implemented using the second "exclude if exceeded" threshold.

2.4 *The DTI-100 VMEbus Interface Unit*

VMEbus Interface Unit (VIU - Figure 2.5) is shown schematically in Figure 2.10.
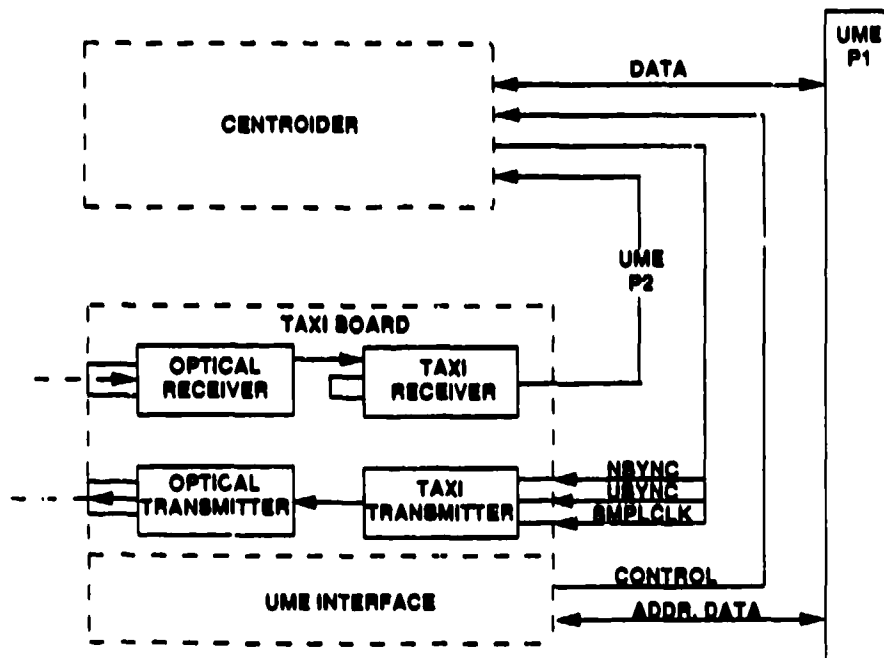
Figure 2.10 VMEbus Interface Unit block diagram.

The VIU provides computer support of the DTI-100 features, including

> threshold set.
> FIFO control and read.
> status monitor: FIFO, Vertical interval, Saturated pixels, Frame #.
> interrupt service: Vertical (V).

11

multiplexor control: Event display and greyscale data.
resync the Taxi links.

The VIU also contains the Taxi control and support. The Taxi transmits H- and V-sync, pixel clock and remote sync to the camera and receives 8 bit digital video together with comp sync and blanking from the camera. Sumitomo® DM-34 optical transmitters and receivers send the camera sync and receive the synchronized 10Mbyte/s video data using glass optical fibers. The remote resync capability is used to synchronize the returning Taxi data link once the outgoing Taxi sync link has achieved lock. This assures fully synchronous, pixel phase locked, operation of the digital video system.

In addition, a video DAC takes the raw 8 bit digital video and composite sync and blanking from the Taxi receiver to produce a RS-170 standard output for diagnostic viewing on a monitor. The VIU also provides 8-bit greyscale data to the Io, Inc. MathCop2 coprocessor for some real-time greyscale video processing applications. The MathCop2 schematic block diagram is shown in Fig. 2.11.
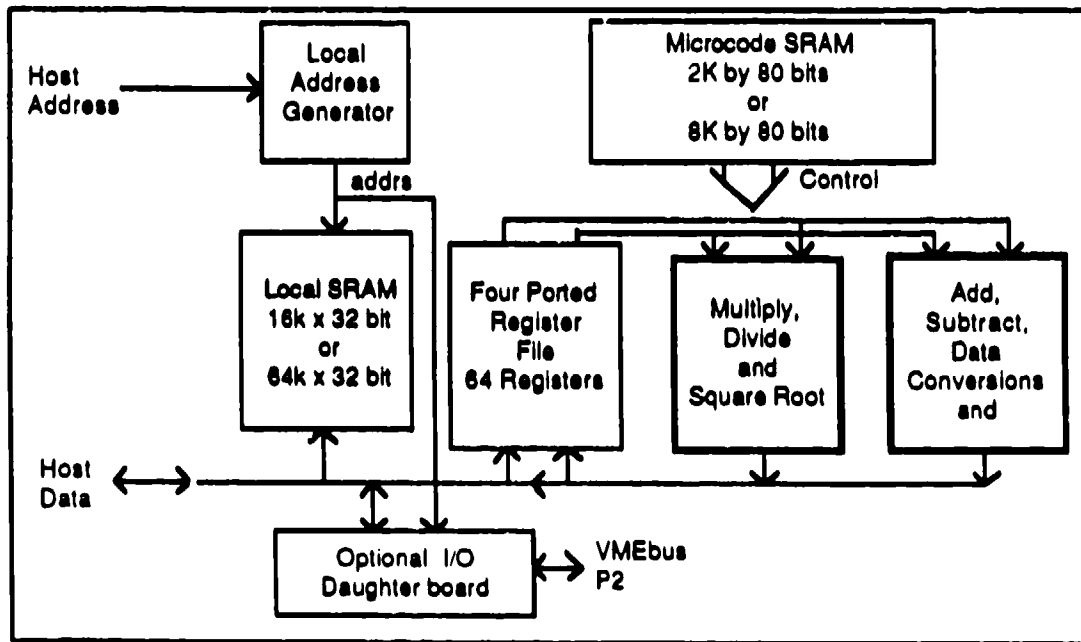
Figure 2.11 MathCop2 coprocessor schematic block diagram.

2.5 Data Logging and Quick-look Capability

The present implementation provides only conventional 9-track magtape for digital data logging. Real-time digital video can be monitored directly from t. ° DTI-100 VIU. Full-frame subtracted digital video and reconstructed event-detected video can be selected for display using a DataCube MaxGraph® video display card.

The math coprocessor allows computation of vector autocorrelations of event data, and can be programmed to provide Knox-Thompson or near-axis triple correlation integrations. It can extract recentered subrasters from greyscale data prior to magtape logging. This considerably reduces the volume of data which must be logged in greyscale mode. This greyscale capability is not yet implemented.

A double-buffered Magtape handler has been written to support the data logging requirements for event detection. The event detection logic cannot effectively accommodate data rates faster than approximately 50K to 70K events/s. Thus conventional 9-track magtape is sufficient for low light level data logging.

A Performance Technologies VMEbus repeater allows the Sun 4/110 graphics workstation, used as system host, to read the real-time digital video system's data buffers. This allows use of any of the data reduction capabilities of the host system to directly access data for near real-time quick look during the course of the observations while at the telescope. This capability is not yet fully implemented.

2.6 *The Sun 4/110 Graphics Workstation Environment*

Development system support is provided by the Sun Microsystems 4/110 graphics workstation. This system has been used for all of the real-time quick-look image reconstruction algorithm development. It will also provide off-line data reductions capability while observing. Software for the realtime system is based on the real-time operating system VxWorks® developed by Wind River Systems. The real-time system software will be down loaded via the VMEbus repeater. The camera system is not dependent upon the workstation for routine operation in event mode. This workstation support is not yet fully implemented.

Ethernet capability exists for future implementation of telescope and instrument support capabilities, as this communication capability is planned for all Steward Observatory telescopes at which this low light level digital video system might be used. No Ethernet capability is available in the stand-alone mode system, as that capability is presently available only through the Sun 4/110 workstation.

For operation at other than Steward Observatory telescopes it is essential that stand alone operation of the real-time data capture system, with quick-look data quality and data quantity monitoring capability, be fully implemented. The development system is required to complete the implementation of that capability.

3. Image Construction Software

For validation of the system in a program of observations, particularly Earth satellite observations, a minimal complement of image construction software is provided. This includes image centroid computation for rapid guiding and telescope control. Simple image phase and image amplitude integration provides the best objects for quick-look evaluation of data qualit and quantity.

3.1 *Event Lists*

To optimize the detector system real-time data logging for low light level work, at low photon rates, data is recorded as a list of the x,y-coordinates of the detected photoelectron events for each frame. The format of the standard event list for a single frame is:

n	(The frame number)
N_n	(Number of events in the frame)
y_1, x_1	(Row, column event coordinates)
y_2, x_2	
...	
y_{N_n}, x_{N_n}	

This repeats for as many frames, M, as are in the file. All of the items in the list are unsigned short integers (16bits). The n-th short exposure image data frame (specklegram) is then

$$i_n(\mathbf{r}) = \sum_{k=1}^{N_n} \delta(\mathbf{r}-\mathbf{r}_k),$$

where the position vector is $\mathbf{r}=(x,y)$ and the event coordinates are $\mathbf{r}_k=(x_k,y_k)$.

3.2 *Rapidguider*

Frame-by-frame recentering, rapid guiding, is the simplest image processing yielding appreciable benefit. The long exposure integration of such recentered data is useful for estimates of seeing necessary for further image construction. In this system rapidguider function is provided by software which determines frame centroids $\mathbf{R}_n = <y>_n, <x>_n$ which can be used for telescope guiding control as well. The long exposure image is then

$$i_L(\mathbf{r}) = \sum_{n=1}^{M} i_n(\mathbf{r}-\mathbf{R}_n).$$

3.3 *Vector Autocorrelator*

The autocorrelation function is accumulated as the two-dimensional histogram of vector differences $\Delta_{ij} = (y_i,x_i)-(y_j,x_j)$ for all pairs of events in the frame. Because this is a raster-readout system, the addresses arrive sorted in raster sequence, so only one half-plane of the centro-symmetric autocorrelation need be computed. These vector autocorrelation histograms are summed for all the frames in the data file. The complete autocorrelation function can then be computed by symmetrical extension. The theory of this is summarized in the "Event Data Reduction Theory," chapter of the **Steward Observatory Speckle Handbook** (Watkins *et al.* 1989). The relevant result is

$$A(\mathbf{r}) = \frac{1}{SM} \sum_{n=1}^{M} \sum_{k=1}^{N_n-1} \sum_{K=k+1}^{N_n} \delta(\Delta_{kK}-\mathbf{r}).$$

$A(\mathbf{r})$ is properly normalized to the (square) array size $S \simeq 2d$, $d=256$ being the detector raster size. The autocorrelation function must be computed in an array twice the effective size of

the detector array. If the speckle camera is operated at magnification great enough to sufficiently oversample the telescope PSF (diffraction pattern), it is possible to reduce the raster size further (to $d=128$) by dividing all raster coordinates by 2.

3.4 Noise Bias Compensation

The raster event detector autocorrelation function, $A(r)$, is biased with a peculiar detector response function. Events are detected as local maxima, produced by photon responses with a significant point spread function localized in the video raster (refer to section 2.3). Therefore, it is impossible to detect events in the same or adjacent pixels (they must be separated by a minimum detectable on at least one pixel). Fig. 3.1 shows an autocorrelation function (ACF) with this peculiar photon event detection point spread function. The crucial signature of this systematic response is the nearest neighbor deficiency surrounding the central response. This example shows the ACF of a point source observed with a double slit mask covering the telescope pupil. The double slit fringe pattern is seen modulating the broad atmospheric seeing response. The corresponding power spectrum (PS), obtained as the Fourier transform of the ACF, is also shown. The characteristic signature of the PS noise bias function (a negative "cosine" function), underlying the double slit aperture response, is clearly seen.
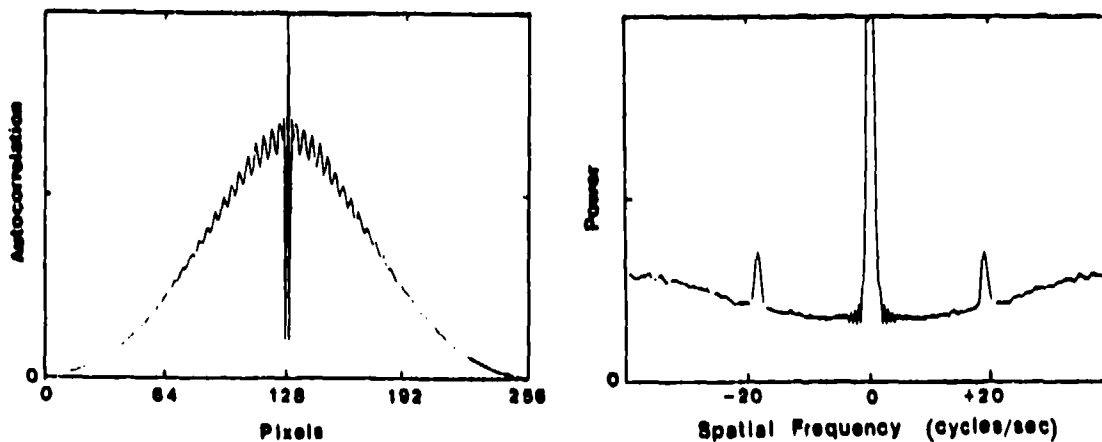
Figure 3.1 ACF/PS pair showing the event noise bias signature of video raster detected events.

This noise bias function must be stable, with invariant shape, in order to be accurately calibrated. The variable magnification, for example, experienced previously with an electrostatically focused four stage system (Hege et al. 1982), yielded a photon detection point spread function which depended upon the position at which the photoelectron event was detected. Such a variable PSF produces a noise bias with seeing and guiding dependent shape which is

15

impossible to calibrate to high precision. This calibratability requirement defines the most stringent constraints of point spread function stability — it must have a stable spatially invariant shape. This in turn establishes the corresponding detector point spread invariance and stability requirements. As shown in Hege et al. 1986, this function must be stable to better than one percent for visibility calibration accuracy of one percent at spatial frequencies up to about 80% of the telescope diffraction limit for a 10th magnitude object. At magnitude 12.5 the requirement is correspondingly 10 times more stringent, etc.

The noise bias function is calibrated by a high signal-to-noise observation of random, uncorrelated photon events uniformly distributed over the detector array. This bias calibration function is scaled to the observed PS at spatial frequencies greater than the diffraction limit, and then subtracted from that PS. Alternatively, models of the PS noise bias may be fit to the PS results using nonlinear least-squares techniques. For further details of such detector noise bias calibrations (see Hege et al. 1986, Christou 1988 and Hege 1989).

3.5 Knox-Thompson cross-correlator

The event address data realization of the Knox-Thompson (K-T) algorithm requires accumulation of the complex cross-correlation quantities

$$\tilde{K}_x(r, s_x) = \frac{1}{SM} \sum_{n=1}^{M} \sum_{\substack{j,k=1 \\ j \neq k}}^{N_n} \exp(-i 2\pi s_x x_k / S) \, \delta(\Delta_{jk} - r)$$

and

$$\tilde{K}_y(r, s_y) = \frac{1}{SM} \sum_{n=1}^{M} \sum_{\substack{j,k=1 \\ j \neq k}}^{N_n} \exp(-i 2\pi s_y y_k / S) \, \delta(\Delta_{jk} - r)$$

The conventional 2 subplane K-T algorithm results from $s_x = s_y = 1$. Ayers et al. 1988 have show that improved performance is possible by extending the method to include more planes (s_x, s_y). We have very limited (16K) cache memory in the MathCop2, hence only the 2 subplane K-T is used for the quick-look capability implemented at this time.

If the photon detection PSF were δ-function like, then omitting the self-correlation terms (for $j = k$) would yield an unbiased estimate of these required cross-spectrum quantities. We have found that non-linear least squares modeling of the bias quantities, as described for the ACF in section 3.4, is a useful approximation for correcting the bias residuals in these cross-spectra.

3.6 Triple-correlator (near-axis subplanes)

Triple-correlation (TC) subplane image constructions using event address data, as implemented by Meng et al. 1989, have been installed and tested in the Sun 4/110 system host. These will not be used for any real-time observing quick-look capability, but they will be available for use at the observing site when the system is operating in hosted mode. The few subplane (2, 3 or 5) TC used for this work is like that described by Northcott et al. 1988.

16

$$\langle J_n^3(f_1, f_2)\rangle_n = FT < \left[\sum_{\substack{m=1 \\ m \neq k, m \neq j}}^{N_a} \exp(-i\,2\pi f_2 \cdot r_m) \times \sum_{k=1}^{N_a} \sum_{j=1}^{N_a} \exp(-i\,2\pi f_2 \cdot r_j)\,\delta(\Delta_{jk} - r) \right] >_n .$$

For 2 subplanes $f_2 = (1,0), (0,1)$. In practice, 3 to 6 subplanes for which $|f_2| < r_o/\lambda S$, known as the near-axis region, which has the highest signal-to-noise ratio, yields a satisfactory result (Meng *et al.* 1989). The ruggedness of the TC process with respect to object complexity suggests that even for real-time applications, where computational efficiency is critical, the generally better performance of the relaxed 2-plane TC algorithm, compared to a 2-plane K-T process, warrants the additional computing effort. Unfortunately, the MathCop2 processor utilized in this realization of the low light level detecting system has insufficient cache memory for implementation of this capability in (near) real-time.

3.7 Simulation studies (AFGL/SO camera data)
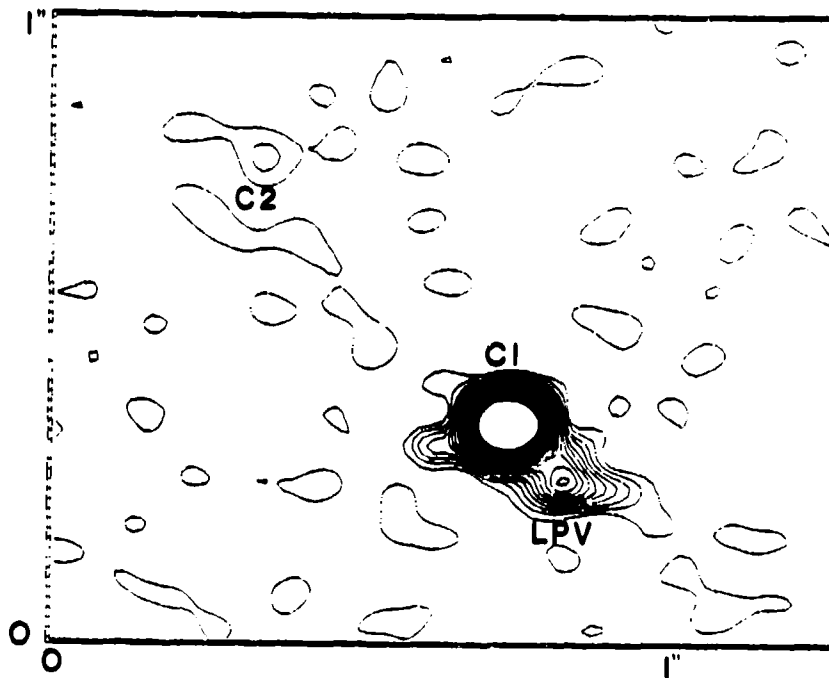
Figure 3.2   R Aqr. Image constructed from AFGL/SO camera data using K-T with Fienup retouching. KPNO 4m telescope. The LPV and H_α emissions are well resolved in this single observation. The labels C1, C2 and LPV indicate the two HII sources and the LPV position as reported from NRAO VLA radio imaging at 2cm (Michalitsianos *et al.*, 1988). The LPV was not completely resolved, and the expected position was plotted from Naval Observatory astrometry. This image shows the LPV as a clearly resolved source component.

Anticipated performance of this **ProxyBlue** based digital video system is based upon experience with the four-stage Varo system utilizing analog recording of video data (Hege *et al.* 1982) and software event detection. During the course of this development effort, algorithm validation using data from that system has produced reassuring results. Fig. 3.2 shows an

image of R Aqr constructed from such AFGL/SO camera data using K-T with Fienup retouching (Fienup 1978). The data was obtained with the KPNO 4m telescope in a 30nm bandpass centered at 656nm (H_α). This result is particularly important as it illustrates that the bias compensation required for phase reconstruction can be accomplished with this type of video raster event detector. The results of this optical high angular resolution image compare favorably with that of the radio VLA, long established as an exemplary high angular resolution imaging facility.

An image of XY Leo was obtained with the same detector and data capture system. In this case, data was obtained using the pathlength compensated Multiple Mirror Telescope in a 30nm bandpass centered at 750nm. Fig. 3.3.
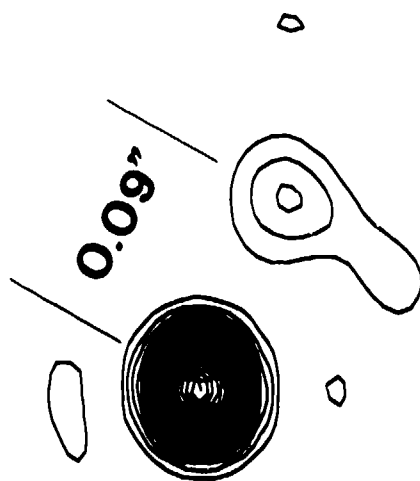
Figure 3.3   XY Leo. Image constructed from AFGL/SO camera data using K-T with Fienup retouching. Multiple Mirror Telescope (Pathlength compensated). The astrometry and photometry are in close agreement with predictions from image models based on spectroscopy (Barden 1987).

This result provides crucial evidence that the image calibration procedures, especially noise bias compensation, can be applied using the coherently cophased MMT. The higher resolution of that 6.8m aperture synsthesis system placed even more stringent requirements on PSF-colored noise bias corrections. The success of this construction for a magnitude 11 object is particularly encouraging.

3.8 *Tests and Validation (MAMA data)*

An important feature of this work is the development and validation of real-time operating capabilities, particularly the quick-look data evaluation capability, for use with any low light level high angular resolution imaging system. The software developed in this project is

intended to be applicable to any photon-counting imaging detector. During this project we have tested our programs with data obtained with the Stanford University MAMA imaging system (Timothy and Morgan 1986). Fig. 3.4 shows data and image constructions for the triple star ADS 11344. The image was constructed from MAMA camera data using Triple Correlation (near-axis $|f_2| \leq 2$ — five subplanes). The SO 2.3m telescope was used for this observation at 650nm, bandpass 30nm.
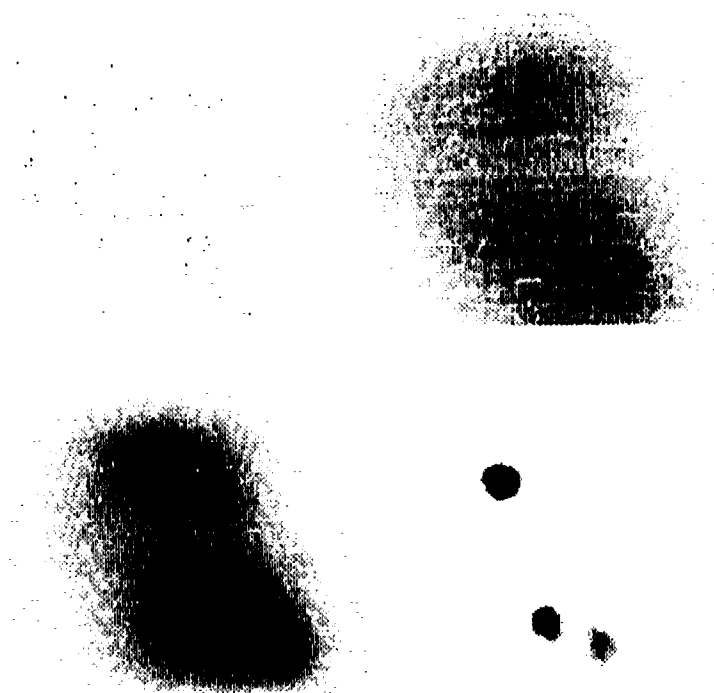
Figure 3.4 ADS11344. These panels represent data taken with a MAMA photon detector. For observing, the real-time raw data display (upper left) is required. The integrated long-exposure (upper right) is useful for verification of camera performance. A simple rapid-guided integration can monitor seeing (lower left), as well as show low-frequency features of a resolved object. The fully-constructed triple star image (lower right) is the desired result. The same data is presented in all four panels.

4. Low Light Level Detecting System Test Results

This describes the tests conducted for each subsystem of the low light level detecting system. The total test program was designed to evaluate the degree to which the hardware and software systems performance meets specified requirements. The test program evaluates five subsystems: Image Intensifier, Camera Electronics, Digital Video System, Host/Interface and Camera Software. *Low light level detecting system observing tests were not completed.*

4.1 *Image Intensifier Tests*

The primary guarantee of successful operation of a photon-counting image intensifier system is the extensive pre-testing program developed during more than a decade of experience in

assembling and testing by R. Cromwell and his associates (Steward Observatory), of high performance, high detective quantum efficiency systems optimized for low light level detection astronomical applications. That experience has yielded the extensive pretesting and assembly testing procedures outlined here. Further details are in Cromwell 1989.

Characterization of Individual Image Intensifier Tubes. Each Proxitronic tube, while operating at 15KV, was evaluated individually for dark emission, field emission, ion dark emissions, signal induced background (number and type of events within a dark spot surrounded by a specified illuminated region), D.C. gain (number of phosphor photons per photoelectron event), photocathode absolute response (or Q.E.) vs. wavelength, uniformity of response, fixed noise characteristics, resolution and geometric fidelity (magnification as function of field radius and fiber optic shear).

Further Testing of First Stage Candidate Tubes. Each candidate first stage tube was further evaluated to determine its pulse power distribution (represented as a histogram of Number of Events vs Event Output Power), photon counting efficiency (% of events which yield a countable response) and dark emission vs. temperature (effects of cooling).

Selection of First Stage Tube. The tube selected as the primary photon detector met or exceeded the following criteria:

a   Dark Emission: Less than 120 $Events \cdot cm^{-2} \cdot sec^{-1}$ (Less than 2 Events/Frame at 60 Hz) at a temperature no cooler than $-30\ °C$.

b   Field Emission: No persistent spots with brightness significantly greater than a single photoelectron response within a 20 mm diameter region in center of detector. No persistent spots brighter than a single ion response anywhere in the detector.

c   Ion Dark Emission: Less than 10 $Events \cdot cm^{-2} \cdot sec^{-1}$ at $-30\ °C$.

d   Ion Signal Induced Background: Less than 10^{-3} Ion/Event within 6 mm diameter uniformly illuminated circular image.

e   D.C. Gain: Greater than 100 530nm X-3 phosphor photons per photoelectron event.

f   Photocathode Quantum Efficiency: The measured response is shown graphically in Fig. 4.1. In any case, the photocathode QE at 550nm must be greater than 10%. Measurements of $mA/watt$ (or percent q.e.) were made at $\lambda = 298.9$, 313.0, 350.0, 380.8, 406.4, 425.6, 497.4, 550.0, 650.0, 750.9, 795.0, 853.0, and 901.9 nm.

g   Uniformity of Response: Less than 5% variation rms from average response at center of tube. In no case peak-to-peak variation greater than 10% over

contiguous regions larger than 100μm dia.

h Fixed Noise Characteristics: No obvious response anomalies, dark spots, etc. upon visual inspection.

i Resolution: Less than 50μm (FWHM). MTF greater than 5% at 20 line-pairs per mm.

j Geometry: Distortion less than 0.1%. Shear less then 30μm.

k Pulse Power Distribution: The tube selected exhibited a well-defined photoelectron event pulse power maximum, well separated from the pulse power distribution of noise events. The pulse power distribution is shown in Fig. 4.2.

l Photoelectron Counting Efficiency: Greater than 90%. This measurement was obtained both as absolute counting efficiency and statistically as the detective quantum efficiency (DQE).

m Dark Emission (Cooled): Dark emission decreases by factor of two for each 7 to 10 °C cooling.
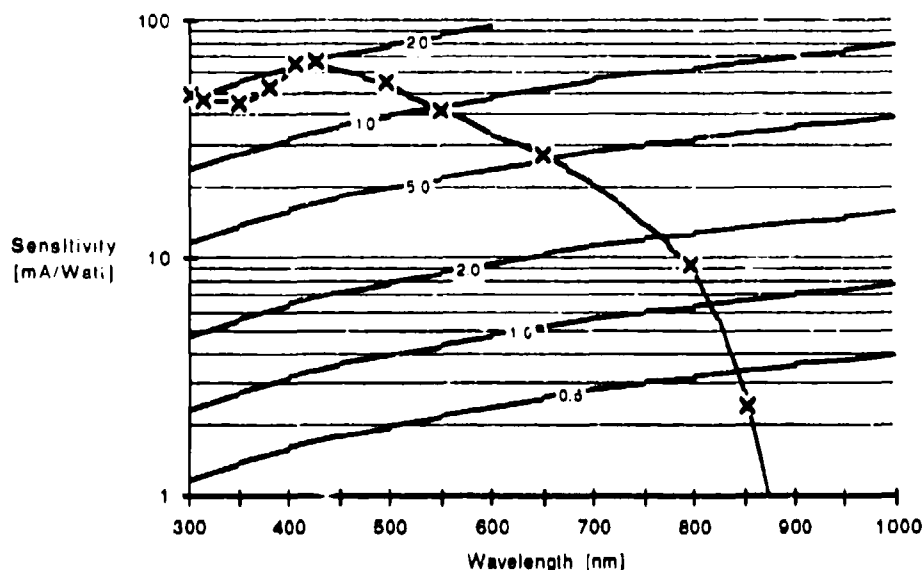
Figure 4.1 Detector Sensitivity. Blue sensitive first stage image detector. The bold curves are for the two tubes selected as satisfying first stage criteria.

21

Selection of Gain Stage Tubes. Acceptable gain stage tubes had less critical dark emission and field emission standards, but had higher D.C. Gain requirements: 1) The D.C. gain must be greater than 400 P-20 phosphor photons per photoelectron event, as demonstrated in Fig. 4.3. 2) The Photocathode Quantum Efficiency for 560nm phosphor photons must exceed 10%. Fig. 4.4 illustrates the typical measured response. All of the other criteria were the same for gain stages as for the first stage.

HV Potted Pairs of Tubes. While operating at 30 KV these image intensifier subassemblies were examined to confirm the expected performance implied by the acceptance criteria of the individual stages. In particular, the potted assemblies showed the expected low noise dark operation, free of field emission effects, and the expected illuminated operation, free of response nonuniformity, with no more than the expected convolution degradation of resolution.

Voltage Divider. The voltage divider must withstand reduced pressure operation equivalent to operation at elevation 14,000 ft. Proper curing of the potting material was verified, with special attention to bonding to leads and tubes, etc. High voltage tests assured reliable operation at 30 KV at the altitude of astronomical observatories.
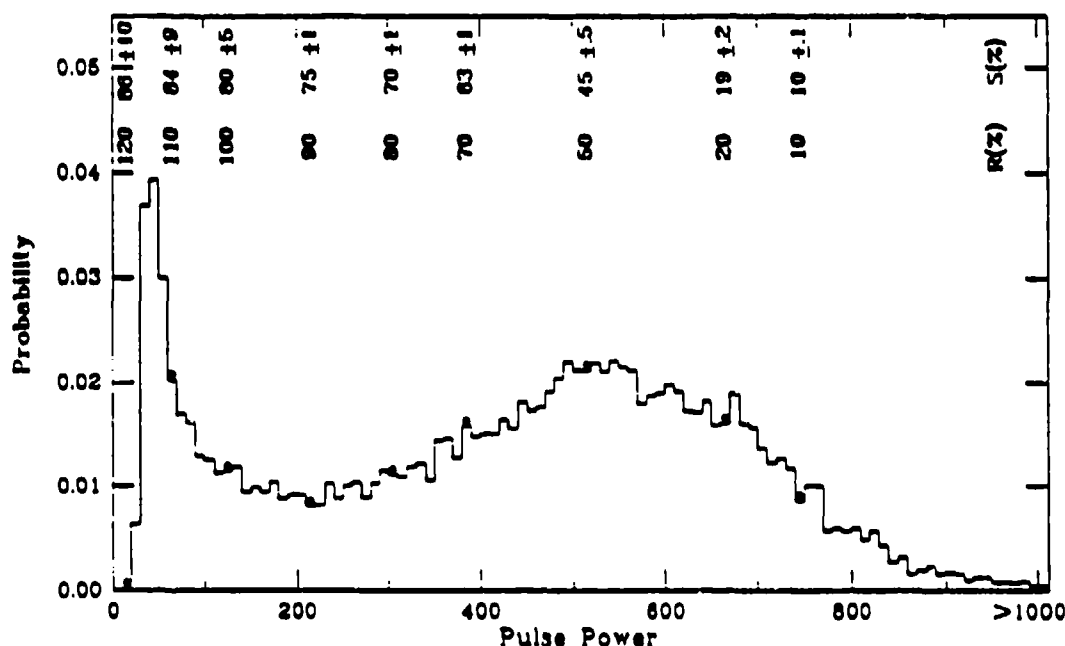
Figure 4.2 Pulse power distribution. The detective sensitivity is shown on the two scales at the top: Upper — computed from signal-to-noise ratios; Lower — computed from absolute counting efficiency. A threshold set at pulse powerr = 200 would allow detection of 90% of the photoelectrons produced at the photocathode.

Fiber Optic Boule. Image Quality: No obvious response anomalies, dark spots greater than 500μm, shears, etc. discovered upon visual inspection. Insulation Quality: Withstands 30 KV with no HV corona or other electrostatic discharge effects. Flatness: Parallel surfaces

are flat to less than 1 µm.
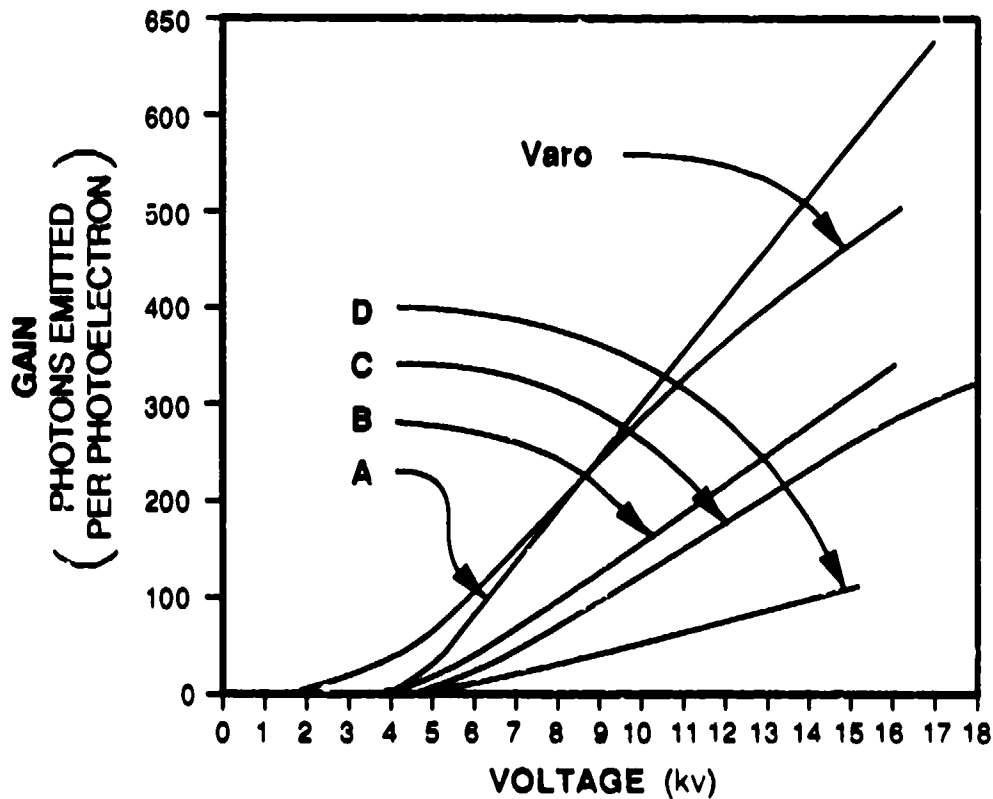
Figure 4.3 D.C. Gain of Image Intensifiers. A is improved Proxitronic gain tube with P-20 phosphor. D is photon-counting Proxitronic tube with X-3 fast phosphor. B and C are earlier Proxitronic P-20 output tubes.

Thermo-Electric Cooler. Heat transfer: $\Delta T = -20\ °C$ at $0\ °C$. Mechanical: Source and sink surfaces flat to within 0.0005 in and parallel to within 1'.

Transfer Lens. This high efficiency transfer lens system consisting of two Kowa lenses, f/0.75 and f/1.4, operated nose-to-nose as a 2:1 image reducer meets the following specifications, referred to a 20 mm diameter field of view (FOV) at the input image plane of the transfer-lens assembly. Resolving power: MTF >5% at 20 line-pairs/mm. Geometric distortion: <0.5% over entire FOV. Efficiency: Vignetting <5% at edge of 20 mm diameter FOV. Light transfer efficiency >7%.

Image Intensifier System Performance. The entire system was evaluated as a unit subject to the same tests at the transfer-lens output as made for the individual tubes. All of the crucial performance criteria were expected to be first stage limited.

It was at this point that the abnormal performance of the system was first noted. When the system was turned on as a unit the first time after the system was fully assembled there was excessive (more than a factor of 100) ion event background. Further, when an image signal was applied, the signal induced background exceeded that originally measured by more than a factor of 100. These are the symptoms of a tube becoming gassy.

23

Considerable effort in reviewing all of the procedures used in system assembly did not reveal any procedural errors which would have compromised the integrity of the seals of the tube. A second candidate tube, which had remained undisturbed in a laboratory drawer during the entire interval from the initial testing until this discovery, was retested and found to be similarly gassy. This pointed to a problem in the manufacture of the tubes, the nature of which has not been fully diagnosed. No significant evidence of gain stage deterioration has been detected, however.
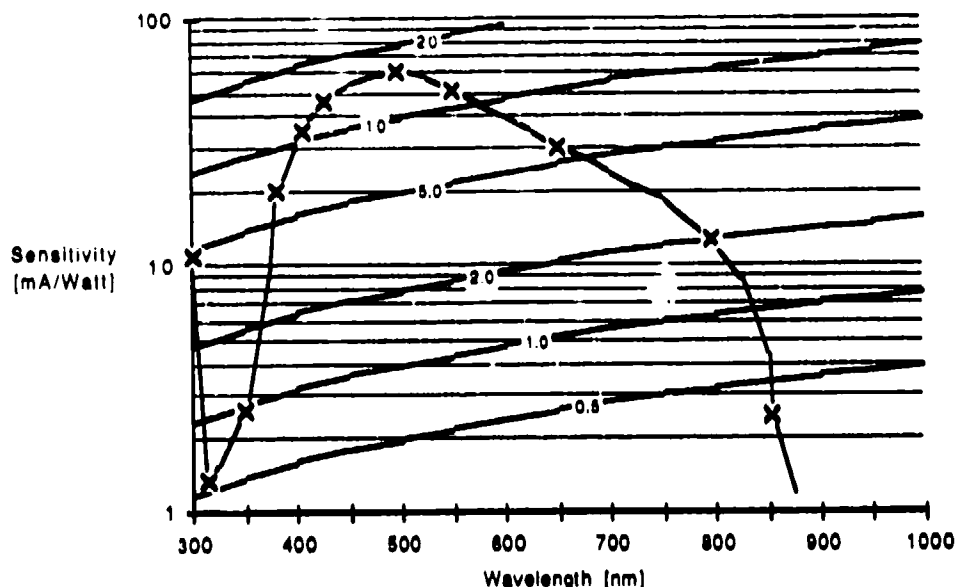
Figure 4.4 Intensifier Sensitivity. A typical gain stage image amplifier is shown. The sensitivity maximum should occur at the phosphor output wavelength, as marked.

4.2 Camera Electronics Tests

In contrast to the battery of tests established by the practitioners of the optoelectronics arts, which are crucial to the success of high performance image intensifier systems, there are fewer pretests involved in selection of digital electronics components. This is because manufacturer's specifications are more easily testable and more reliably deliverable, and there is more flexibility in replacing a substandard component in the finished product. Therefore, these test procedures focused upon the confirmation of specified functions of the assembled system. These tests confirmed the design validity, accuracy of fabrication into subassemblies, and specification-consistent performance of integrated circuit amplifier, digitizer, logic and memory components. The tests specified here concentrated upon demonstration of valid electronics subsystem performance. They do not constitute a rigorous automated test procedure for detection and analysis of failure.

24

Digital Video Camera. An important feature of this digital video design is the assurance of the lowest noise pick-off of the most linear video signal from the CCD video sensor. Because this output still contains clock contamination, the following tests assured that the mode of camera operation and the signal extraction and preprocessing are optimized for lowest noise with maximum linearity.

a   Repeat-field operation: Verified odd lines only.

b   Linearity of analog response: Less than 1% rms deviation ($\gamma=1$). *Final calibration requires integrated system. This test is not completed.*

c   Analog noise measurement: Less than 1/256 (±1 LSB) of linear dynamic range (rms). *Quantitative validation requires integrated system. The video system was used successfully for the tests of the assembled image intensified output. Qualitatively the system performs as expected.*

d   A/D validation: Expected linear video ramp and video camera test chart tests: Linear to ±1/2 LSB and two pixel resolution of test chart. *This was to be measured with the integrated system.*

e   Pixel synchronization: The A/D sample and hold is properly in phase with CCD clock, and the latched A/D output is properly in phase with the Taxi clock (The "1/3-pixel" problem: 606.66/line has been adequately controlled).

Fiber Optic Taxi (Video Synchronization and Digital Data) Links. The parallel/serial/parallel optical fiber synchronization and data link has reliably provided synchronization of the digital video processor to the CCD video sensor from the master clock and accurately return the 8-bit digitized video data from the CCD sensor with correct pixel registration in more that 50 hrs of operation on the laboratory bench.

a   Valid synchronization and stable transmit and receive of Taxi clocks is maintained at 120 MHz. The clocks are jitter-free to less than ±0.5ns. The reset signal reliably establishes data-word framing.

b   Data test bits applied at Taxi data transmitter are accurately and reliably received and decoded at Taxi data receiver.

c   Digitized CCD video data (test pattern) is accurately in phase with the Taxi transmitter pixel clock. Absolute address offset of integrated system is 5 pixels.

d   8-bit video test patterns are received at the DVP noise free. This validates all fiber optics cable connections as well sync and data Taxi performance.

e   Taxi clock phase is adjusted so that the received valid data is registered with the video logic clock to within ±70ns (<2/3 pixel) when examined at any pixel along any video raster line.

DTI-100 Test Signal Generator. Tests of the DTI-100 digital filter and photoelectronic event discriminator and locator (DVP) required construction and validation of specialized test equipment. This device generates digital video data rasters with specific patterns. The patterns required are 1) a single modulated intensity dot at any specified pixel along any selected line and 2) DIP switch and jumper controlled sets of modulated intensity dots in separated or adjacent pixels. This device simulates the characteristics of photoelectron events to be detected and localized by the DTI-100. Performance validation requires use of a general purpose video line analyzer. The following test situations are generated:

a   Field synchronous modulated dot generator test: A pixel, amplitude modulated over 8 fields, produced at a selected location.

b   Multiple dot generator tests: Two dots, as above separated by a known vector.

c   Fat-pixel generator: Produces modulated event patterns which occupy more than one pixel.

DTI-100 Performance Validation. The following tests verified DTI-100 performance.

a   Pixel synchronization in event detector logic unit is valid.

b   Digital filter (512 pixel/line to 256 pixel/line): produces valid sums with valid pixel pairing.

c   Both 1 line delay and 2 line delay valid.

d   Full-frame subtract (Memory test -- Stationary image subtracts fo zero, Moving image is detected). Temporal detection is valid.

e   Event Threshold/Frame Localization: Correct unique spatial detection of peak dot generated by test circuit.

f   Event peak location: Fat-dot test detects and correctly locates event at highest raster pixel.

g   Differential Greyscale: Valid frame-subtracted video is produced.

h   *The digital video multiplexor has not yet been tested.*

i   Event Address detection is valid and correctly buffered. Column adr. valid. Row adr. valid.

j   Saturated pixel are correctly counted.

This event detection logic appears to accurately locate events in the output of the image intensifier as well as for the test circuit. *We await image tube repairs to verify performance with a faintly illuminated image test pattern.*

4.3 *Digital Video System Host/Interface Tests*

An existing VMEbus 68000 CPU camera controller system was used for laboratory tests of the operating modes of the DTI-100 digital video processor, to monitor its status, to set the event detection threshold level and to provide video interrupt driven data logging of photoelectron event data. *Neither 8-bit pixel greylevel data logging nor digital video data processing control has yet been verified.*

Digital Video Processor (DVP) Interface. Test software has been written to verify the following functions of the DVP interface.

a   Read DVP status words.

b   Select DVP operating mode.

c   Set Threshold Level.

d   FIFO control and Event data buffering.

e   Video interrupt (V) service (frame control).

f   8-bit greyscale readback.

g   Saturated pixel readback.

h   Taxi Reset.

All of these functions operate as expected. *Software for D/A video monitor support is not yet complete.*

Io MathCop2. Operation as specified by Io, Inc. using Io, Inc. supplied test procedures and software is verified. This includes proper execution of test routines, proper execution of data reduction subroutines, including ACF accumulation. These tests were conducted in a borrowed MC68020 VMEbus system. *Operation of real-time video MathCop2 interface to DTI-100 digital video module has not yet been tested.*

27

Interface drivers to control camera functions, to move data to buffers, processors and magtape and to control image processing functions have been written in FORTH for the MC68000 real-time host used in these camera tests. These are constructed of calls to the subroutines required for video system host/interface validation. These can be easily transliterated to C when the fully integrated system is completely implemented.

Data Acquisition Program Initialization. The buffers, files and devices are properly initialized. *No observing software has yet been tested.*

Faint Object Observing Mode (Photoelectron Events). The routine which selects event-mode camera operation, sets video threshold, initializes math coprocessor and awaits command to initialize data acquisition has been tested in the laboratory. The user is prompted for data header information, including photoelectron event threshold and data file identification. Reads telescope interface and logs observing particulars in header. The program verifies initiation of valid photoelectron event data acquisition, logging and on-line processing upon user command.

No bright object observing mode (Differential Greyscale) software has yet been tested. This observing mode will be required at signal rates such that photoelectron event discrimination becomes ambiguous in single video fields. It must have two submodes of operation, unshuttered and shuttered. The shuttered mode is required when signal strength is sufficiently great that peak fluxes of more than one photon per pixel are detected in a single video frame.

4.5 *Low Light Level Detecting System Observing Tests*

These tests have not yet begun because the extensive laboratory tests of the fully integrated low light level detecting systems, required before field testing at the telescope can begin, are not yet complete.

5. Conclusions and Recommendations

Steward Observatory has designed and constructed a photon-counting imaging detector and image integration system optimized for the special requirements of low light level optical interferometric imaging at visible wavelengths using the Knox-Thompson algorithm. Laboratory evaluation of the completed system shows the need for further image intensifier development.

5.1 *Summary of System Performance*

The testing of the completed four stage Proxitronic image intensifier system showed that the first image intensifier stage has drastically deteriorated in the interval between the time it was selected as the tube of choice for that first stage and the time it was first turned on as a fully assembled system. This is based upon acceptance tests showing that when it was received

from Proxitronic it had a photon counting efficiency in excess of 80% of the diode's photocathode efficiency, and in all regards met the first stage performance requirements. This should have produced imaging with overall photon counting efficiency of 15% at its sensitivity peak near 400nm. The system is presently not usable, however, due to excessive signal induced ion event background which was not seen in the original laboratory tests.

No mishandling in fabrication or in thermal cycling during testing has been identified. It is also significant that a second nearly identical tube, which had remained in a drawer in the laboratory during the entire 18 month interval, has also failed in a similar way. There seems to have been some failure common to both tubes causing them to become gassy. The gain stages, which are significantly different in construction — being optimized for gain rather than for single event detection — appear not to have deteriorated.

Digital video CCD readout of the transfer lens coupled image intensifier output in 240 × 256 format is provided at 60Hz frame rate. The bidirectional fully synchronous fiber optic digital data link which allows control and operation of the telescope mounted image detector and video digitizer system appears to be entirely satisfactory. Full frame subtraction provides the expected image intensifier lag suppression. CCD pixel synchronous operation has been verified.

The video event detection logic localizes photoelectron responses to a unique pixel in a particular frame. An ion event exclusion threshold capability has not, however, solved the problem with the noisy first intensifier stage (the ion event rate is too excessive for compensation by such simple means).

Double buffered magtape data logging provides loss-free data logging at the maximum rate at which a 1600bpi 75ips 9 track magtape system can write. Full 8 bit greyscale images can also be recorded, raw or with frame subtraction, on 9 track tape.

The math coprocessor algorithms to provide real-time frame centroiding and autocorrelation function accumulation have been tested successfully. This will provide much needed quick-look data evaluation during observation at the telescope. For conventional Lab speckle interferometry, this is tantamount to real-time data reductions. The computing bandwidth is sufficient to provide 2 plane Knox-Thompson cross correlation accumulation. However, the cache memory in the present math coprocessor is inadequate to contain these complex quantities at the full 240 × 256 resolution of the detector.

A Sun Microsystems workstation is provided for system development and for observing-time support of the real-time detector system. This Sun 4/110 development system also supports statistics- and diffraction-limited image construction with fully validated software for off line Knox-Thompson and triple correlation algorithms.

The system has not yet been fully tested and evaluated for deep space imaging tasks using the coherently cophased (path-length compensated) Multiple Mirror Telescope. These tests have not been attempted because of the deteriorated image intensifier first stage.

The most significant obstacle to the successful completion of this low light level detector system is the considerable image intensifier work which is essential to correct the deficiencies of the present first stage. There are several tasks required to repair, maintain and further improve this photon counting and analog imaging system. These are fairly well-understood tasks which can be completed in relatively short time.

The following image intensifier acceptance-testing and installation tasks, involving purchase of two first stage Proxitronic X-3 tubes, one first stage 25mm ITT P-47 proximity focus tube and three gain stage Proxitronic tubes, should begin immediately.

The Proxitronic first stage tubes are for immediate replacement and backup of the present first stage tubes, both of which were discovered to become surprisingly gassy, full of ion emission and ion signal-induced background, after an interval of time. A new tube should perform as well as the original tubes. The backup tube should be ordered after the acceptance and installation of the replacement tube as immediate insurance to keep the system up and running. Additional electron scrubbing of the screen, during manufacturing, may help prevent (or significantly delay) the tubes from becoming gassy.

Another company besides Proxitronic should also be encouraged to demonstrate the capability to provide the high-level performance intensifiers needed in this project. A distinct advantage in ITT is that they are ultimately capable of providing tubes larger than 25mm diameter, with 40mm and 80mm packages being standard fare for ITT, and even larger diameters are possible. ITT claims to now have the capability of producing high counting efficiency P-47 phosphors that are blackened to prevent scattered light. Earlier we had rejected ITT because at that time the blackening process was found not sufficiently developed.

The additional gain stage intensifiers from Proxitronic will serve as insurance in case further experience with the gain stages shows that they too become gassy with time. This precaution should also be an immediate priority because of the long lead time for delivery and acceptance testing of these select tubes.

There also seems to be more developmental work required which will take more time to complete. These longer range tasks would involve the development of alternate technologies to provide the low geometrical distortion, low signal-induced background, high resolution and high electron counting efficiency first stage tubes required for this work. This may involve further development of electrostatic tubes with blackened P-47 phosphor, with a back scattered electron trap electrode, and in 10mm format. These developments should also include investigations of alternative phosphor screens having high electron counting efficiency, rapid response time, and a more peaked and narrower pulse power distribution than that of existing phosphors.

Other technologies which should be investigated include a 40mm, minimum, diameter proximity focused diode with fiber optic input and output faceplates and rapid P-47 phosphor for use as a second stage intensifier. This is to serve as a preamplifier that may be required between a front stage and a microchannel plate gain stage in order to maintain a tight pulse power

distribution in a high counting efficiency system.

We also argue the need for development of a good red-response photocathode. Our success with Proxitronic in developing a good blue-response bialkali and multialkali photocathode has been encouraging. We need now to accomplish the same success in the red (around 700nm to 800nm). Fine-tuned multialkali photocathodes should be developed by Proxitronic and by ITT. For a magnetic focused tube, a III-V photocathode could show special promise (QE > 20% at 800nm).

6. References

Ayers, G.R., M.J. Northcott and J.C. Dainty, "Knox-Thompson and Triple-correlation Imaging through Atmospheric Turbulence," *J. Opt. Soc. Am. A* **5**, 963-985, 1988.

Barden, S.C., "Detection of a BY Draconis-like Binary Companion to the Contact Binary XY Leonis," *Astrophys. J.* , pp 333-342, 1987.

Beckers, J.M., E.K. Hege and H.P. Murphy, "The differential speckle interferometer," *Proc. SPIE* **445**, *Instrumentation in Astronomy V*, pp 462-468, 1983.

Christou, J.C., "Application of Speckle Interferometry Techniques: Working with Real Data," in *High-resolution Imaging by Interferometry, Part I*, Ed. F. Merkle, 15-18 March 1988, pp 97-111, ESO Conference and Workshop Proceedings No. 29, Garching bei München, F.R.G., 1988.

Cromwell, R.H., "Gain, Pulse Power Distribution and Single Electron Counting Efficiency of P-20, P-47 and X-3 Phosphors," Final Scientific and Technical Report, Sep 86 — Dec 88, prepared for Navy Ocean Systems Center N66001-86-C-03111/P00004, Steward Observatory, August 1989.

Fienup, J.R., "Reconstruction of an Object from the Modulus of its Fourier Transform," *Opt. Lett.* **3** 27-29, 1978.

Harvey, D.A., "A selection of Earth orbiting satellite targets for speckle interferometric imaging," Steward Center for Orbital Mechanics, Steward Observatory, November 1988.

Hege, E.K., E.N. Hubbard, P.A. Strittmatter and W.J. Cocke, "The Steward Observatory Speckle Interferometry System," *Optica Acta*, **29**, 701-715, 1982.

Hege, E.K., and P.R. Vokac, "Real-time Amplitude and Phase Integration for Diffraction Limited Imaging," *Proc. SPIE* **627**, *Instrumentation in Astronomy VI*, pp 780-786, 1986.

Hege, E.K., A. Eckart and J.C. Christou, "The Noise Bias Problem in Optical Speckle Imaging," *ibid*, pp 772-779, 1986.

Hege, E.K., "Notes on Noise Calibration of Speckle Imagery," in *Diffraction-Limited Imaging with Very Large Telescopes*, D.M Alloin and J.-M. Mariotti (eds.), pp 113-124, Kluwer Academic Publishers, 1989.

Meng, J., G.J.M. Aitken, E.K. Hege, and J.S. Morgan, "Triple-correlation subplane reconstruction of photon-address stellar images," submitted to *J. Opt. Soc. Am. A*, September 1989.

Michalitsianos, R.J., R.J. Oliversen, J.M. Hollis, M. Kafatos, H.E. Crull and R.J. Miller, "R Aquarii: The Large-scale Optical Nebula and the Mira Variable Position," *Astron. J.* **95**, pp 1478-1483, 1988.

DISTRIBUTION LIST

addresses	number of copies
RADC/OCSP ATTN: Paul L. Repak Griffiss AFB NY 13441-5700	12
University of Arizona Steward Observatory ATTN: Dr. E. Keith Hege Tucson, AZ 85721	3
RADC/DOVL Technical Library Griffiss AFB NY 13441-5700	1
Administrator Defense Technical Info Center DTIC-FDA Cameron Station Building 5 Alexandria VA 22304-6145	5
Defense Advanced Research Projects Agency 1400 Wilson Blvd Arlington VA 22209-2308	2
the Optical Sciences Co Attn: Dr. David Fried P. O. Box 1329 Placentia, CA 92670	1
SAIC Attn: Dr. Frederick Gebhardt 1040 Waltham Street Lexington, MA 02173	1
W.J. Schafer Associates ATTN: Dr. Peter Ulrich 1901 Fort Meyer Drive Arlington, VA 22209	1

```
WL/AR-1                                                    1
ATTN: Dr. C. B. Hogge
Kirtland AFB, NM 87117-6008


Adaptive Optics Associates                                 1
ATTN: Dr. Larry Schumtz
54 Cambridge Park Drive
Cambridge, MA 02140


HQ AF Space Command/XPD                                     1
ATTN: Col. R. Benedict
Peterson AFB, CO 80914-5001


Lockheed Missiles and Space Co.                            1
Document Management
ATTN: Dr. R. Lytell
3251 Hanover Street
Palo Alto, CA 94304


AVCO Research Laborartory                                   1
ATTN: Dr. P. McCormick
P.O. Box 261
Puunene, HI 96784


Naval Sea Systems Command                                   1
PMS-405-200
ATTN: John Albertine
Washington DC 20362-5101


M.I.T Lincoln Laboratory                                    1
ATTN: Dr. C. Primmerman
P.O. Box 73
Lexington, MA 02173


SDIO-TDE                                                    1
Pentagon
ATTN: LCDR J. Garner
Washington, DC 20301-7100


RADC (OL-AB)                                                1
c/o AVCO Research Labs
ATTN: Maj. T. Zych
P.O Box 261
Puunene, Maui, HI 96784
```

```
AFWAL/AAWW-3                                    1
ATTN: Mr. George Vogel
Wright-Patterson AFB, OH 45433-6543


DARPA/DEO                                       1
ATTN: Dr. Shen Shey
1600 Wilson Boulevard
Arlington, VA 22209


WL/ARBA                                         1
ATTN: Dr. Robert Fugate
Kirtland AFB, NM 87117


Naval Sea Systems Command                       1
Dept of the Navy
ATTN: CDR F. Marcell
PMS-405-200
Washington, DC 20362-5101

Lawrence Livermore National Labs                1
ATTN: Burt Massie
Mail Station L495
P.O. Box 808
Livermore, CA 94550

RADC/ESE                                        1
ATTN: Dr. Freeman Shepard
Hanscom AFB, MA 01731


MIT Lincoln Laboratory                          1
ATTN: Dan Hermann
244 Wood Street
Lexington, MA 02173


W.J Schafer Associates                          1
ATTN: Dr. Daniel Leslie
1500 Wilson Blvd.
Arlington, VA 22209


W. J. Schafer Associates                        1
Suite 205
2000 Randolph Road, SE
Albuquerque, NM 87106
```

AVCO Research Laboratory   1
ATTN: Steven Heising
Suite 109
4410 E. Fountain Road
Colorado Springs, CO 80916

The Jet Propulsion Laboratory   1
ATTN: Dr. Aden Meinel
4800 Oak Grove Drive
PAsadena, CA 91109-5000

Science Applications International   1
   Corporation
ATTN: John J. Vasselli
199 Liberty Plaza, Suite 200
Rome, NY 13440

SD/CNSC   1
ATTN: Mr. Ron Thompson
P.O. Box 92960
Los Angeles, CA 90009-2960

Hughes Aircraft Corporation   1
EDSG Bldg E-55
ATTN: Dr. Wilbur Brown
P.O. Box 902
El Segundo, CA 90245

ERIM   1
Advanced Concepts Division
ATTN: Richard Paxman
P.O. Box 8618
Ann Arbor, MI 48107

FTD/SDMSY   2
ATTN: Capt. Felicia Ansty
Wright-Patterson AFB, OH 45433-6508

U. S. Army Lab. Command   1
Atmospheric Sciences Lab
ATT: Dr. Robert Rubio
SLCAS-AS-D
WSMR, NM 88002

WL/ARC   1
ATTN: Major James W. O'Connor
Kirtland AFB, NM 87117-6008

```
AFSTC/SWS                                             1
ATTN: Steven Harrington
Kirtland AFB, NM 87117-6008


Jet Propulsion Laboratory                             1
ATTN:  Dr. B. Martin Levine
MS-169/314
4800 Oak Grove Drive
Pasadena, CA   91109

HQ WL/ARBC                                            1
ATTN: Mr. Ron Sessions
Kirtland AFB, NM 87117-2308


DARPA                                                 1
ATTN: DR. H. Lee Buchanan
1400 Wison Blvd.
Arlington, VA 22209-2308


The Jet Propulsion Laboratory                        1
ATTN: Mr. Philip Moynihan
4800 Oak Grove Drive
Pasadena, CA 91109-5000


MIT/LL                                                1
ATTN: Dr. Georgette Burgess
P.O. Box 73
Lexington, MA 02173-0073


Naval Air Development Center                          1
ATTN: Mr. Michael Hess
Code 3011
Warminster, PA 18974-5000


OSAF                                                  1
ATTN: Maj. Gary Dahlen
The Pentagon
Washington, DC 20330-5000


SDIO/SN                                               1
ATTN: Dr. Walter Wells
Washington, DC 20301-7100
```

HQ AFSPACECOM/XPDD   1
ATTN: Col Rettig P. Benedict, Jr.
Peterson AFB, CO 80914-5001

W.J. Schafer Associates   1
ATTN: R.W. Dyer
200 Liberty Plaza
Rome, NY 13440

University of Arizona   1
Steward Observatory
ATTN: Dr. E. Keith Hege
Tucson, AZ 85721

MISSION

of

Rome Air Development Center

RADC plans and executes research, development, test and selected acquisition programs in support of Command, Control, Communications and Intelligence (C^3I) activities. Technical and engineering support within areas of competence is provided to ESD Program Offices (POs) and other ESD elements to perform effective acquisition of C^3I systems. The areas of technical competence include communications, command and control, battle management information processing, surveillance sensors, intelligence data collection and handling, solid state sciences, electromagnetics, and propagation, and electronic reliability/maintainability and compatibility.